UC Berkeley
UC Berkeley Previously Published Works

Title
Thermal conductance of strongly bonded metal-oxide interfaces

Permalink
https://escholarship.org/uc/item/3nm848fv

Journal
Physical Review B, 91(11)

ISSN
2469-9950

Authors
Wilson, RB
Apgar, Brent A
Hsieh, Wen-Pin
et al.

Publication Date
2015-03-01

DOI
10.1103/physrevb.91.115414

Peer reviewed

Thermal conductance of strongly bonded metal-oxide interfaces

R. B. Wilson,[1,*] Brent A. Apgar,[1,2,3] Wen-Pin Hsieh,[1,4] Lane W. Martin,[1,2,5] and David G. Cahill[1]

[1]*Department of Materials Science and Engineering and Materials Research Laboratory, University of Illinois, Urbana, Illinois 61801, USA*
[2]*Department of Materials Science and Engineering, University of California, Berkeley, Berkeley, California 94720, USA*
[3]*International Institute for Carbon-Neutral Energy Research, 744 Motooka, Nishi-ku, Fukuoka 819-0395, Japan*
[4]*Institute of Earth Sciences, Academia Sinica, Nankang, Taipei 11529, Taiwan*
[5]*Materials Science Division, Lawrence Berkeley National Laboratory, Berkeley, California 94720, USA*

We report the results of time-domain thermoreflectance (TDTR) measurements of two strongly bonded metal-oxide systems with unusually large thermal conductances. We find that TDTR data for the epitaxial $SrRuO_3/SrTiO_3$ interface is consistent with an interface conductance $G > 0.8\,\mathrm{GW\,m^{-2}\,K^{-1}}$. For an Al/MgO interface at a pressure of 60 GPa, we find $G \approx 1.1\,\mathrm{GW\,m^{-2}\,K^{-1}}$. Both are within 40% of the maximum possible conductance for these systems, as predicted by simple theory.

PACS number(s): 44.10.+i, 65.40.−b, 66.70.−f

I. INTRODUCTION

Thermal transport properties of bulk crystals are determined by the interplay of three characteristics: translational symmetry, atomic bonding strength, and chemical composition [1]. Near an interface, all three of these characteristics are dramatically altered compared to a bulk material and therefore thermal transport near an interface can be severely impeded [2]. Consequently, the thermal properties of nanostructured materials and nanoscale devices are often dominated by the transport properties of interfaces [3].

Thermal transport across an interface between two crystals is often described with an interfacial thermal conductance G, that relates the heat current at the interface to the temperature drop at the interface, $J = G\Delta T$. When heat is transported by phonons, the transport coefficient is often assumed to be [4]

$$G = \frac{1}{4}\sum_j \int t_\omega v_\omega c_\omega d\omega_j. \tag{1}$$

Here, t_ω, v_ω, and c_ω are properties for phonons of frequency ω_j on one side of the interface where j labels polarization; t_ω is the probability of transmission, v_ω is the group velocity, and c_ω is the heat capacity per frequency, $c_\omega = \hbar\omega D_\omega \partial n_\omega/\partial T$, where D_ω is the density of states and n is the Bose-Einstein distribution function. According to Eq. (1), the maximum interface conductance an isotropic material can possess with another material G_{max} occurs when $t_\omega = 1$ for all thermally excited vibrational modes and is limited by the rate that thermal energy in the material can impinge on a crystallographic plane. As we have defined it here, G_{max} is determined solely by the phonon dispersion relation of a single material and therefore is a material-specific property, not an interface-specific property. The maximum conductance for an interface between two specific materials is restricted by detailed balance to be less than or equal to the value of G_{max} that is lowest for the two materials. Values for G_{max} are typically on the order of $1\,\mathrm{GW\,m^{-2}\,K^{-1}}$ and are linearly correlated with the product of a material's Debye velocity and volumetric heat capacity, $v_D C$ (see Fig. 1).

Observed values of G range between $G_{max}/100 < G < G_{max}/2$, because t_ω is less than unity for a significant fraction of phonon frequencies in most real interfacial systems [3–13]. Factors that cause the average value of t_ω to be significantly less than unity have been well documented [3,5]. A significant level of interfacial disorder [5–7], interfacial roughness [8], weak interfacial bonding [9,10,13], or drastic differences in the vibrational frequencies of the two constituent materials [11] all result in values of G that are significantly lower than G_{max}. Because the vast majority of reported interfacial thermal conductance values are for systems where some, or all, of these four factors are present, it remains unclear whether G can ever approach or exceed G_{max}. In other words, the intrinsic limits to G that result from material properties of the constitutive materials, such as phonon dispersion, are not yet clear because relatively few systems with clean and strongly bonded interfaces have been studied. The highest previously reported values of G at room temperature are 620 and $700\,\mathrm{MW\,m^{-2}\,K^{-1}}$ for the epitaxial GaN/AlN and TiN/MgO systems [14,15], approximately 40% lower than G_{max} for GaN and TiN (Fig. 1). Progress toward a complete microscopic understanding of G requires additional measurements of systems with clean and strongly bonded interfaces.

Here, we describe the results of two experiments that, in different ways, examine how closely G can approach G_{max}. Both experiments focus on systems where the interfacial bonding can be expected to be strong.

In our first set of experiments, we report the results of time-domain thermoreflectance (TDTR) measurements of G for epitaxial $SrRuO_3/SrTiO_3$. Both the $SrTiO_3$ and $SrRuO_3$ possess perovskite crystal structures with alternating layers of SrO and TiO_2 (for $SrTiO_3$) and SrO and RuO_2 (for $SrRuO_3$) along [001]. Therefore, the $SrRuO_3/SrTiO_3$ system has strong interfacial bonds, a commensurate chemical structure, and commensurate bonds on both sides of the interface, with a lattice mismatch of only 0.6% at room temperature [16–18]. Transmission electron microscopy studies demonstrate that pulsed-laser-deposited $SrRuO_3$ thin films can possess coherent and chemically abrupt interfaces with an underlying oxide substrate [19,20]. In short, the $SrRuO_3/SrTiO_3$ system possesses close to a model interface.

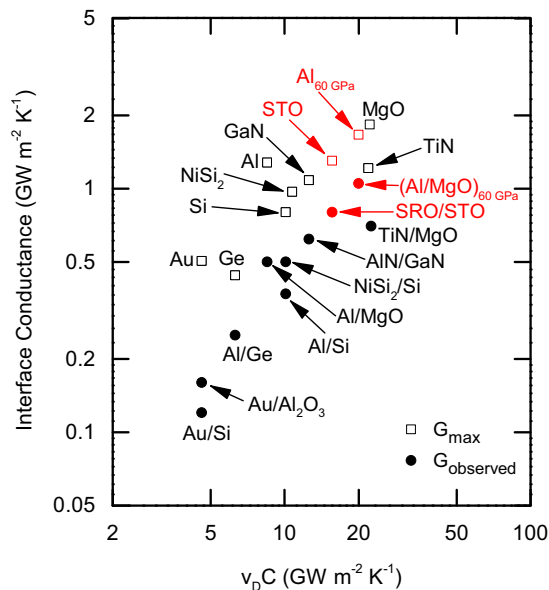*Corresponding author: wilson81@illinois.edu

FIG. 1. (Color online) Comparison between the highest reported thermal conductances for various materials (filled circles) to the theoretical maximum conductances predicted by Eq. (1) (open squares). Red markers indicate the results of this study. Interface conductance data is strongly correlated to the product of the Debye velocity and heat capacity (x axis). Conductance data is only shown for studies that took steps to produce a relatively clean interface, such as an *in situ* high-temperature bake prior to metal deposition. Data for G of Au/Al_2O_3 is from Ref. [4], $NiSi_2/Si$ from Ref. [12], Au/Si from Ref. [13], TiN/MgO from Ref. [14], AlN/GaN from Ref. [15], and Al/Ge and Al/Si data are from Ref. [40].

In our second set of experiments, we report TDTR measurements of G for Al/MgO between 0 and 60 GPa. High-pressure measurements ensure stiff interfaces with strong atomic bonds [21]. Additionally, the reduction in lattice constant and stiffening of elastic constants with increasing pressure [22] allow us to systematically study how G compares to G_{max} across a range of $v_D C$ values.

The values of G we deduce from TDTR measurements of $SrRuO_3/SrTiO_3$ and Al/MgO at 60 GPa are the two highest interface conductance values reported to date. Our TDTR measurements of $SrRuO_3/SrTiO_3$ samples are consistent with $G \geqslant 0.8 \, \mathrm{GW \, m^{-2} \, K^{-1}}$, approaching our estimates of $G_{max} \approx 0.8$ and $1.3 \, \mathrm{GW \, m^{-2} \, K^{-1}}$ for $SrRuO_3$ and $SrTiO_3$, respectively. For Al/MgO at 60 GPa we find $G \approx 1 \, \mathrm{GW \, m^{-2} \, K^{-1}}$, within 40% of our estimate of $G_{max} \approx 1.7 \, \mathrm{GW \, m^{-2} \, K^{-1}}$ for Al at 60 GPa.

II. METHODS

Thin films of $SrRuO_3$ with thicknesses between 8 and 170 nm were grown from a ceramic $SrRuO_3$ target via pulsed laser deposition using a KrF excimer laser (LPX 205, Coherent). The $SrRuO_3$ films were grown on etched and annealed [20] TiO_2-terminated $SrTiO_3$ (001) substrates from Crystec GmbH, held at 600 °C in 100 mTorr of oxygen pressure. X-ray diffraction, x-ray reflectivity, spectroscopic ellipsometry, and four-point probe characterizations were performed on all $SrRuO_3$ films immediately following growth and immediately prior to the TDTR measurements.

The electrical resistivity of the $SrRuO_3$ films varied between 220 and 240 $\mu\Omega$ cm. No correlation between film thickness and electrical resistivity was observed in the thickness range studied herein, indicating boundary scattering is not an important source of resistance in these $SrRuO_3/SrTiO_3$ samples. Rutherford backscattering confirmed a stoichiometric Sr to Ru ratio of 1.01 ± 0.03.

The thermal transport properties of the $SrRuO_3/SrTiO_3$ samples were characterized with TDTR using the metallic $SrRuO_3$ film as an optical transducer [23]. In TDTR, the thermal response of a sample to a train of pump pulses periodically modulated at frequency f is observed by measuring temperature-induced changes in the intensity of a reflected probe beam. Experimental data consists of the in-phase and out-of-phase voltages recorded by a Si photodiode connected to an rf lock-in that picks out the signal components at the pump modulation frequency f. The measured signal is compared to the predictions of a thermal model that uses the thermal properties of the sample as inputs. Unknown thermal properties are adjusted until the predictions of the thermal model agree with the experimental data. In our analysis, the heat capacity and thermal conductivity of $SrTiO_3$ was fixed to $2.74 \, \mathrm{J \, cm^{-3} \, K^{-1}}$ based on literature values and $11.5 \, \mathrm{W \, m^{-1} \, K^{-1}}$ based on TDTR measurements of Al-coated $SrTiO_3$ substrates [24,25]. The thermal conductivity of $SrRuO_3$ was fixed to $5.0 \pm 0.5 \, \mathrm{W \, m^{-1} \, K^{-1}}$ based on TDTR measurements of an Al-coated 170-nm $SrRuO_3$ film. The product of the $SrRuO_3$ film thickness and heat capacity per unit volume (hC) and the $SrRuO_3/SrTiO_3$ interface conductance G were treated as fitting parameters.

Our standard thermal model for interpreting TDTR data assumes that the laser energy is deposited at the metal film surface and that the intensity fluctuations of the probe beam are proportional to the metal film's surface temperature [26]. Both of these assumptions are invalid for TDTR measurements that use the thin $SrRuO_3$ films as the optical transducer because the optical penetration depth of $SrRuO_3$ is 50 nm at the pump/probe wavelength of 785 nm [23], which is larger than the film thickness. Therefore, we made several changes to our standard thermal model when analyzing the TDTR data collected from bare $SrRuO_3/SrTiO_3$ samples. First, instead of assuming that the measured signal is proportional to surface temperature of the metal film, we follow Ref. [27] and assume it is proportional to a weighted average of the temperature profile through depths below the surface. The weighting function is calculated from an optical model for the thermoreflectance dR/dT vs film depth using optical constants and thermo-optic coefficients measured via spectroscopic ellipsometry [23]. Second, instead of assuming the heat was deposited at the metal surface, we used a bidirectional model that deposits the heat at a plane on the interior of the metal film some distance z from the surface. A description of how we adapt our thermal model to accommodate bidirectional heat flow from the heated plane can be found in the Appendix of Ref. [28]. We then calculate the thermal response of the sample with $z = (n + 1/2)h/10$ for $n = 0–9$, where h is the thickness of the $SrRuO_3$ film. Finally, we compare a weighted average of the thermal responses for $n = 0–9$ to the experimental data, with the spatial derivative of the Poynting vector used as the weighting function.

For the measurements of the Al/MgO interface conductance at high pressure, we prepared a clean Al/MgO interface by coating an epi-polished MgO (001) crystal from SPI Supplies with an Al film via dc magnetron sputtering. Prior to the *in situ* Al deposition, the MgO crystal was heated under high vacuum ($<5 \times 10^{-8}$ Torr) for 30 min to 1200 K in order to provide as clean an interface as possible. The TDTR measurements were performed in a symmetric piston-cylinder diamond anvil cell with Ar as a pressure medium. Further details of our experimental and thermal modeling methods for performing TDTR measurements in a diamond anvil cell can be found in Refs. [21] and [22].

III. RESULTS

TDTR measurements of thick SrRuO$_3$ films have small sensitivity to G because at film thickness greater than 30 nm, the thermal resistance intrinsic to the SrRuO$_3$ film is larger than the interfacial thermal resistance, $h/\Lambda_{SRO} \gg G^{-1}$. Unfortunately, for SrRuO$_3$ films less than 30 nm the reflectance of the SrRuO$_3$/SrTiO$_3$ sample is sensitive to the optical constants of SrTiO$_3$. To determine the minimum SrRuO$_3$ film thickness required to prevent the temperature response of the underlying SrTiO$_3$ substrate from affecting the TDTR signal, we performed TDTR measurements on bare SrRuO$_3$/SrTiO$_3$ samples with thicknesses between 8 and 49 nm.

Representative TDTR data for a 16-nm SrRuO$_3$ sample is shown in Fig. 2(a). At pump-probe delay times less than 10 ps, the measured signal is sensitive only to the thermal effusivity of the substrate and the heat capacity per unit area of the metal
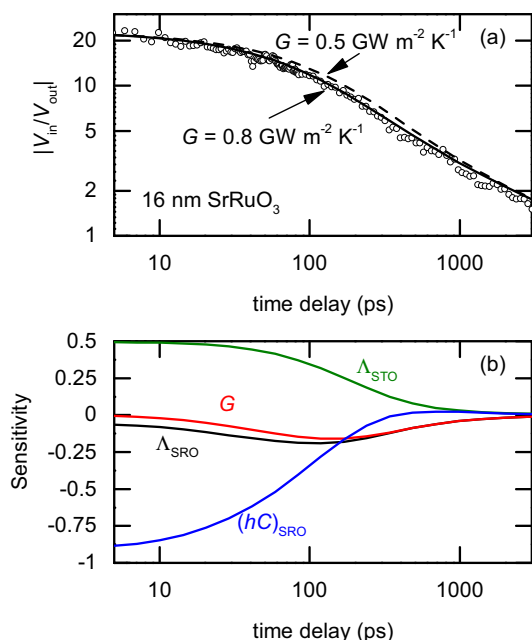

transducer (hC). At pump-probe delay times ranging from 50 ps to 2 ns, the decay rate of the signal is also sensitive to G and the thermal conductivity of the SrRuO$_3$ [see Fig. 2(b)]. In Fig. 3(a), we compare the TDTR-derived value for (hC) of seven films between 8 and 49 nm to $(1 - x)(h_{XRR} C_{SRO})$, where h_{XRR} is the film thickness via x-ray reflection (XRR) measurements, C_{SRO} is the literature value for the heat capacity of SrRuO$_3$ of 2.86 J cm^{-3} K^{-1} [29], and $(1 - x)$ is a pinhole correction factor. Atomic force microscopy (AFM) scans of the 9-, 12-, 16-, 23-, 26-, and 28-nm SrRuO$_3$/SrTiO$_3$ samples revealed pinhole surface area coverages of $x = 0.08$, 0.03, 0.02, 0.02, 0.003, and 0.003, respectively, which reduces the heat capacity per unit area of these samples. For film thicknesses larger than 12 nm, TDTR-derived values of (hC) are in agreement with $(1 - x)(h_{XRR} C_{SRO})$. We conclude that for SrRuO$_3$ film thicknesses larger than 12 nm, the thermal response of the SrTiO$_3$ substrate is not an important contributor to the measured signal.

In order to determine G from a TDTR measurement, we fixed (hC) to the TDTR-derived value and calculated the mean-square deviation between the prediction of our thermal model and our TDTR data for G between 0.1 and 10 GW m^{-2} K^{-1} [see Fig. 3(b)]. (We do not include the 49-nm film in this figure because the interface conductance is an insignificant thermal resistance in this sample.) In order to account for the fact that the sensitivity decreases with increasing G and increasing h, we normalized the mean-square deviation by the maximum sensitivity of $V_{in}(t)/V_{out}(t)$ to G [see Fig. 3(c)]. For the calculation shown in Figs. 3(b) and 3(c), since we are determining a lower bound for G, we fixed the thermal conductivity of the SrRuO$_3$ film to $\Lambda_{SRO} = 5.5$ W m^{-1} K^{-1}, the upper limit of our confidence interval. Considering the sensitivity weighted best-fit values of G for the 16-, 23-, 25-, and 28-nm SrRuO$_3$ films, we estimate a lower limit for G of 0.8 GW m^{-2} K^{-1}.

Any artifact in the signal caused by SrRuO$_3$ transparency will be most severe for the thinnest films. The best-fit value for G increases with increasing thickness. Therefore, we conclude that any artifacts due to transparency decrease the apparent G and are not the source of the unusually large value of G for SrRuO$_3$/SrTiO$_3$ that we observe.

After performing TDTR measurements of the bare SrRuO$_3$/SrTiO$_3$ samples, we coated the 16- and 28-nm-thick SrRuO$_3$ films with an Al film approximately 80 nm thick and conducted additional TDTR measurements. Both sets of TDTR data for the Al-coated samples are consistent with an interface conductance for Al/SrRuO$_3$ of 0.17 GW m^{-2} K^{-1} $\pm$10%. The addition of the Al/SrRuO$_3$ interfacial conductance to the heat-transfer problem significantly reduces the impact of the SrRuO$_3$/SrTiO$_3$ interface conductance on the decay rate of the sample surface temperature in comparison to measurements of bare SrRuO$_3$ films. For example, the maximum sensitivity of our TDTR data to the SrRuO$_3$/SrTiO$_3$ interface conductance is reduced by a factor of 6 for the 16-nm SrRuO$_3$ sample, from 0.16 to 0.028. Therefore, the addition of the Al film makes our measurements an inferior probe of G for the SrRuO$_3$/SrTiO$_3$ interface. Our thermal model predictions are in agreement with the TDTR measurements of the Al-coated SrRuO$_3$ samples as long as the model input for the SrRuO$_3$/SrTiO$_3$ interface conductance exceeds

FIG. 2. (Color online) Time-domain thermoreflectance (TDTR) measurement of the SrRuO$_3$/SrTiO$_3$ interface. (a) Example TDTR data for the 16-nm SrRuO$_3$ thin film along with the predictions of our thermal model. (b) Corresponding sensitivity parameters as a function of delay time. The peak sensitivity to G is −0.16 at a delay time of $t = 150$ ps. This means that a 10% variation in G will produce a 1.6% variation in the ratio signal at $t = 150$ ps.
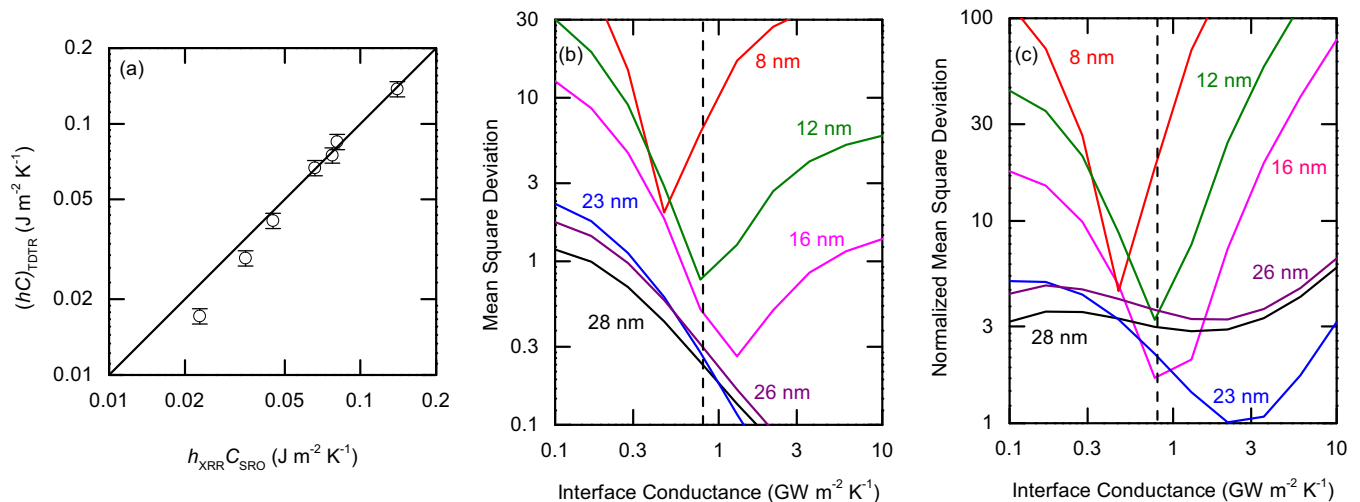
FIG. 3. (Color online) (a) Comparison of the TDTR-derived value for the heat capacity of the SrRuO$_3$ film per unit area (hC) to the value derived from x-ray reflectivity measurements of film thickness. At thicknesses above 12 nm the two measures of the film heat capacity per unit area are in agreement, indicating the TDTR measurement is robust despite the fact that the SrRuO$_3$ films are not optically opaque. (b) Mean-square deviation between the predictions of the thermal model and the TDTR data as a function of G. (c) Normalized mean-square deviation between thermal model predictions and TDTR data. Each point on each mean-square deviation curve is normalized by the TDTR signal's maximum sensitivity to G for that x-axis value of G. The curves were normalized in this way to account for the decreasing measurement sensitivity to G with increasing G. The dashed vertical line at 0.8 GW m^{-2} K^{-1} represents our estimate of the lower bound conductance that is consistent with our TDTR measurements.

0.5 GW m^{-2} K^{-1}. Using the same criteria as we used in Fig. 3(c), the best fit occurs at 0.65 GW m^{-2} K^{-1}.

In comparison to the SrRuO$_3$/SrTiO$_3$ data, interpretation of the Al/MgO TDTR data is relatively straightforward because
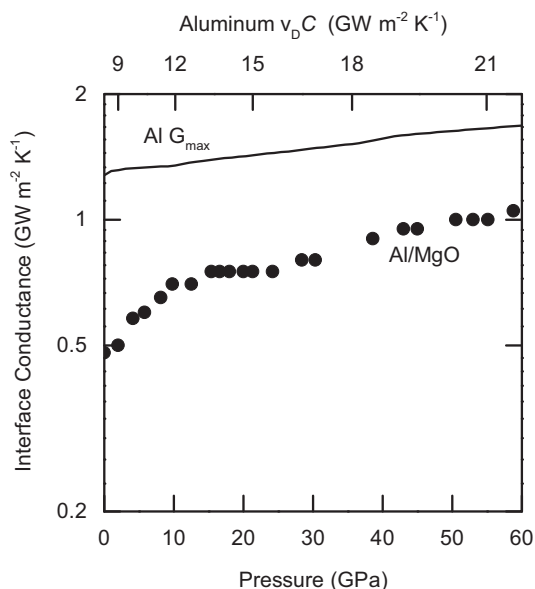

FIG. 4. Pressure dependence of the thermal conductance of an Al/MgO interface. The top axis shows how the product of Debye velocity and heat capacity of Al increases with pressure. At pressures less than 10 GPa, G increases with pressure more rapidly than our prediction for G_{max} of Al, suggesting an increase in the average phonon transmission coefficient due to the stiffening of interfacial bonding with pressure. Above 10 GPa, G increases at approximately the same rate as our prediction for G_{max}. At 60 GPa, the conductance of Al/MgO is within 40% of the maximum predicted by Eq. (1).

the sensitivity to the interface conductance in a metal/MgO system is high and easily distinguishable from other thermal properties [14]. Figure 4 shows the pressure dependence of G for the Al/MgO system. For a range of pressure between 0 and 60 GPa, $v_D C$ for Al increases by a factor of 2.5 from 8.5 to 22 GW m^{-2} K^{-1}. Between 0 and 10 GPa, the interface conductance of Al/MgO increases by over 40%, while $v_D C$ and G_{max} for Al only increase by 30% and 5%, respectively. From 20 to 60 GPa, G of Al/MgO increases by $\approx 25\%$, while $v_D C$ and G_{max} increase by 35% and 20%, respectively. That G increases much more rapidly with pressure than G_{max} below 10 GPa suggests that the average transmission coefficient t_ω is increasing due to an increase in interfacial bonding strength and stiffness [21]. This result is mildly surprising since the MgO was heated to 1200 K under high vacuum immediately prior to Al deposition in order to remove surface contamination, suggesting that interfacial stiffness is an influential parameter for interfacial conductance, even when the interface is relatively clean.

IV. ANALYSIS AND DISCUSSION

To estimate G_{max} using Eq. (1), we approximated the group velocity of the acoustic phonons as

$$\frac{\partial \omega_j}{\partial q} = v_j - 2 \left(\frac{v_j q_D - \omega_M}{q_D^2} \right) q, \qquad (2)$$

where j labels either the longitudinal or transverse phonon branches, q is the wave vector, $q_D = (6\pi^2 n)^{1/3}$, where n is the volumetric unit-cell density, and ω_M is the maximum frequency for a wave vector in the [100]. Equation (2) yields a dispersion relation that is a second-order polynomial that converges to ω_M near the zone boundary. For the optic

TABLE I. Material properties used to estimate the maximum conductance predicted by Eq. (1). Acoustic longitudinal and transverse speeds of sound, v_L and v_T, are calculated from elastic constants using the averaging scheme outlined by Ref. [42]. The zone-boundary acoustic and optic frequencies are taken from phonon dispersion data.

Property	Au	Ge	Al	Si	NiSi$_2$	GaN	SrTiO$_3$	Al (60 GPa)	MgO	TiN
v_L (km/s)	1.7[a]	3.4[b]	6.5[c]	9.6[d]	6.9[e]	8.6[f]	8.5[g]	15[h]	10[i]	10.4[j]
v_T (km/s)	3.3[a]	5.4[b]	3.3[c]	5.6[d]	3.1[e]	5.2[f]	5.2[g]	7[k]	6.4[i]	6.1[j]
f_L (THz)	4.5[l]	7[m]	10[n]	12[m]	7.5[e]	9[o]	4[p]	17[h]	13[q]	10[r]
f_T (THz)	2.5[l]	2.4[d]	6[n]	5[m]	4[e]	6.5[o]	3.6[p]	11[h]	8.6[q]	8[r]
$v_{O,L}$ (km/s)		−0.8	−1.6	1.2	−1.6		2, 2, 1.8, −1		−2.5	1.2
$v_{O,T}$ (km/s)		−0.5	−1	−0.9	0		3.5, 2.3, 1.5, −1.5		0.7	0.7
$f_{O,L}$ (THz)		7.4	13	11	23		8.7, 11, 17, 20		17	19
$f_{O,T}$ (THz)		7.9	14	7.7	17		5.6, 10, 10, 14		13	17

[a]Reference [43]; [b]Ref. [44]; [c]Ref. [45]; [d]Ref. [46]; [e]Ref. [47]; [f]Ref. [48]; [g]Ref. [49]; [h]Ref. [50]; [i]Ref. [51]; [j]Ref. [52]; [k]Ref. [53]; [l]Ref. [30]; [m]Ref. [54]; [n]Ref. [55]; [o]Ref. [56]; [p]Ref. [57]; [q]Ref. [58]; [r]Ref. [59].

phonons, we assume a linear dispersion relation and calculate the group velocity via a best fit to the neutron-scattering measurements of the dispersion relation in high-symmetry directions. Table I provides the material properties used to calculate the values of G_{max} shown in Fig. 1.

To test how accurate of an approximation Eq. (2) is for cubic crystals, we calculated G_{max} for Al and Au with several other dispersion relations. Using a Born–von Karman force constant model [30,31] to calculate the phonon frequencies and group velocities across the entire Brillouin-zone results in G_{max} for Al and Au of 1.3 and 0.6 GW m^{-2} K^{-1}, in good agreement with the values of 1.3 and 0.5 GW m^{-2} K^{-1} we derived using Eq. (2). For comparison, a Debye approximation for the dispersion relation yields 2.1 and 1.1 GW m^{-2} K^{-1} for G_{max} of Al and Au, a truncated Debye model of the type used in Ref. [32] yields 0.8 and 0.3 GW m^{-2} K^{-1} for G_{max} of Al and Au, and a sine-type dispersion of the type used in Ref. [33] yields 0.8 and 0.4 GW m^{-2} K^{-1} for G_{max} of Al and Au. Finally, using separate sine-type dispersion approximation for the longitudinal and transverse branches yields 0.9 and 0.5 GW m^{-2} K^{-1} for G_{max} of Al and Au. We conclude that Eq. (2) is an accurate approximation for the dispersion relation of acoustic phonons in cubic materials.

Our calculation of G_{max} includes all optic phonon branches. The value derived for G_{max} is insensitive to whether we approximate the experimental dispersion relations of optic branches with linear curves, higher-order polynomials, or numerically interpolated curves. However, for the SrTiO$_3$ optic phonons, the isotropic assumption appears to be less robust than for acoustic phonons. For SrTiO$_3$, assuming isotropic dispersion relations for the optic phonons that replicate the dispersion curves in exclusively the [100], [110], or [111] yields G_{max} values of 1.1, 1.1, or 1.6 GW m^{-2} K^{-1}, respectively. The linear approximation for the optic branches of SrTiO$_3$ provided in Table I describes dispersion curves that split the differences between these three directions, therefore yielding a G_{max} of 1.3 GW m^{-2} K^{-1}.

Experimental data for the phonon dispersion relation of SrRuO$_3$ are not available, precluding us from confidently estimating G_{max} for SrRuO$_3$. Given that the ratio of $v_D C$ for SrRuO$_3$ to $v_D C$ for SrTiO$_3$ is 0.6, a crude estimate for G_{max} of SrRuO$_3$ is 0.8 GW m^{-2} K^{-1}, corresponding to 0.6 of G_{max} for SrTiO$_3$. Alternatively, assuming the phonon dispersion relation of SrRuO$_3$ at room temperature is well approximated by the [100] and [010] dispersion relations of SrRuO$_3$ in its ferromagnetic ground state, as calculated by Miao *et al.* via first principles [34], yields a G_{max} value of 0.7 GW m^{-2} K^{-1}.

In the present work, we have limited our analysis to systems where the interfacial bonding can be expected to be reasonably strong because both theoretical and experimental studies have demonstrated that weak interfacial bonding can severely impede interfacial heat flow [9,10,21,35–37]. In other words, weak interfacial bonding significantly lowers the probability that phonons that impinge on an interface will transmit to the other side, thereby resulting in a value for G that is determined by the microscopic details of the interface and not the two constituent materials. Alternatively, several theoretical studies have predicted that the transmission probability can be reduced by a small amount if the stiffness of interfacial bonds is made larger than the stiffness of the bonds of the two constituent materials [35,36]. To our knowledge, a reduction in G due to overly stiff interfacial bonds has not been experimentally observed.

Despite large values of G for SrRuO$_3$/SrTiO$_3$ and (Al/MgO)$_{60\,GPa}$ that are near G_{max}, we cannot conclude that the average interfacial transmission coefficient t_ω approaches unity for the majority of heat-carrying phonons because the derivation of Eq. (1) approximates the phonon occupation of all phonons with an equilibrium phonon distribution on both sides of the interface [38,39]. Equation (1) is only an accurate description of thermal transport across an interface at position z if $T(z - \ell_\omega) - T(z + \ell_\omega) \approx \Delta T$, where ΔT is the temperature drop at the interface and ℓ_ω is the average mean-free path of a phonon of frequency ω [40]. In other words, $G_{max}\Delta T$ is not the largest possible heat current at the interface if a significant fraction of heat-carrying phonons ballistically traverse a significant temperature drop in the material prior to transmitting across the interface. The approximation $T(z - \ell_\omega) - T(z + \ell_\omega) \approx \Delta T$ is valid if $\ell_\omega \ll L_K$, where the Kapitza length $L_K = \Lambda/G$ is the distance across which the temperature drop in the material will equal the temperature drop at the interface. For large values of G, i.e., $G \approx 1$ GW m^{-2} K^{-1}, $\ell_\omega \ll L_K$ is likely unsatisfied for a significant fraction of

heat-carrying phonons, meaning J_ω may exceed $t_\omega v_\omega c_\omega \Delta T /4$ for a significant fraction of phonon frequencies.

In conclusion, identifying the limits to the interface conductance that are intrinsic to the constituent materials, and not intrinsic to properties of the interface, is an important step towards a complete microscopic understanding of interfacial thermal transport. We have defined a simple material property $G_{\max}$ that is a useful tool for estimating the interface conductance of strongly bonded systems (see Fig. 1). In general, the TDTR measured conductances of the clean interfaces compiled in Fig. 1 lie in a relatively narrow range, $0.3 G_{\max} < G < 0.7 G_{\max}$. (Au is an exception, likely due to electron-phonon resistance near the interface [28,41].) We characterized the thermal conductance of two strongly bonded interfaces, $SrRuO_3/SrTiO_3$ at ambient pressure and Al/MgO at high pressure. Both interfaces have unusually high thermal conductances.

[1] J. M. Ziman, *Electrons and Phonons* (Oxford University Press, Amen House, London, 1960).

[2] E. T. Swartz and R. O. Pohl, Rev. Mod. Phys. **61**, 605 (1989).

[3] D. G. Cahill, P. V. Braun, G. Chen, D. R. Clarke, S. Fan, K. E. Goodson, P. Keblinski, W. P. King, G. D Mahan, A. Majumdar, H. J. Maris, S. R. Phillpot, E. Pop, and L. Shi, Appl. Phys. Rev. **1**, 011305 (2014).

[4] R. J. Stoner and H. J. Maris, Phys. Rev. B **48**, 16373 (1993).

[5] P. E. Hopkins, ISRN Mechanical Engineering **2013**, 19 (2013).

[6] T. Beechem, S. Graham, P. Hopkins, and P. Norris, Appl. Phys. Lett. **90**, 054104 (2007).

[7] W. Ih Choi, K. Kim, and S. Narumanchi, J. Appl. Phys. **112**, 054305 (2012).

[8] P. E. Hopkins, L. M. Phinney, J. R. Serrano, and T. E. Beechem, Phys. Rev. B **82**, 085307 (2010).

[9] M. D. Losego, M. E. Grady, N. R. Sottos, D. G. Cahill, and P. V. Braun, Nat. Mater. **11**, 502 (2012).

[10] P. J. O'Brien, S. Shenogin, J. Liu, P. K. Chow, D. Laurencin, P. H. Mutin, M. Yamaguchi, P. Keblinski, and G. Ramanath, Nat. Mater. **12**, 118 (2013).

[11] H.-K. Lyeo and D. G. Cahill, Phys. Rev. B **73**, 144301 (2006).

[12] D. Liu, R. Xie, N. Yang, B. Li, and J. T. L. Thong, Nano Lett. **14**, 806 (2014).

[13] D. W. Oh, S. Kim, J. A. Rogers, D. G. Cahill, and S. Sinha, Adv. Mater. **23**, 5028 (2011).

[14] R. M. Costescu, M. A. Wall, and D. G. Cahill, Phys. Rev. B **67**, 054302 (2003).

[15] Y. K. Koh, Y. Cao, D. G. Cahill, and D. Jena, Adv. Funct. Mater. **19**, 610 (2009).

[16] J. M. Albina, M. Mrovec, B. Meyer, and C. Elsässer, Phys. Rev. B **76**, 165103 (2007).

[17] D. G. Schlom, L.-Q. Chen, X. Pan, A. Schmehl, and M. A. Zurbuchen, J. Am. Ceram. Soc. **91**, 2429 (2008).

[18] L. W. Martin and D. G. Schlom, Curr. Opin. Solid State Mater. Sci. **16**, 199 (2012).

[19] L. Äkäslompolo, A. M. Sánchez, Q. H. Qin, A. Hakola, T. Kajava, and S. van Dijken, Appl. Phys. A **110**, 889 (2013).

[20] G. Koster, L. Klein, W. Siemons, G. Rijnders, J. S. Dodge, C.-B. Eom, D. H. Blank, and M. R. Beasley, Rev. Mod. Phys. **84**, 253 (2012).

[21] W.-P. Hsieh, A. S. Lyons, E. Pop, P. Keblinski, and D. G. Cahill, Phys. Rev. B **84**, 184107 (2011).

[22] D. A. Dalton, W.-P. Hsieh, G. T. Hohensee, D. G. Cahill, and A. F. Goncharov, Sci. Rep. **3**, 2400 (2013).

[23] R. B. Wilson, B. A. Apgar, L. W. Martin, and D. G. Cahill, Opt. Express **20**, 28829 (2012).

[24] Y. Suemune, J. Phys. Soc. Jpn. **20**, 174 (1965).

[25] *Thermophysical Properties of Matter*, edited by Y. S. Touloukian (Plenum, New York, 1970), Vol. 2.

[26] D. G. Cahill, Rev. Sci. Instrum. **75**, 5119 (2004).

[27] G.-M. Choi, R. B. Wilson, and D. G. Cahill, Phys. Rev. B **89**, 064307 (2014).

[28] R. B. Wilson, J. P. Feser, G. T. Hohensee, and D. G. Cahill, Phys. Rev. B **88**, 144305 (2013).

[29] S. Yamanaka, T. Maekawa, H. Muta, T. Matsuda, S.-i. Kobayashi, and K. Kurosaki, J. Solid State Chem. **177**, 3484 (2004).

[30] J. W. Lynn, H. G. Smith, and R. M. Nicklow, Phys. Rev. B **8**, 3493 (1973).

[31] G. Gilat and R. M. Nicklow, Phys. Rev. **143**, 487 (1966).

[32] D. T. Morelli, J. P. Heremans, and G. A. Slack, Phys. Rev. B **66**, 195304 (2002).

[33] C. Dames and G. Chen, J. Appl. Phys. **95**, 682 (2004).

[34] N. Miao, N. C. Bristowe, B. Xu, M. J. Verstraete, and P. Ghosez, J. Phys.: Condens. Matter **26**, 035401 (2014).

[35] D. A. Young and H. J. Maris, Phys. Rev. B **40**, 3685 (1989).

[36] C. B. Saltonstall, C. A. Polanco, J. C. Duda, A. W. Ghosh, P. M. Norris, and P. E. Hopkins, J. Appl. Phys. **113**, 013516 (2013).

[37] M. Shen, W. J. Evans, D. Cahill, and P. Keblinski, Phys. Rev. B **84**, 195432 (2011).

[38] J. A. Katerberg, C. L. Reynolds, and A. C. Anderson, Phys. Rev. B **16**, 673 (1977).

[39] G. D. Mahan and F. Claro, Phys. Rev. B **38**, 1963 (1988).

[40] R. B. Wilson and D. G. Cahill, Nat. Commun. **5**, 5075 (2014).

[41] A. Majumdar and P. Reddy, Appl. Phys. Lett. **84**, 4768 (2004).

[42] O. L. Anderson, J. Phys. Chem. Solids **24**, 909 (1963).

[43] Y. A. Chang and L. Himmel, J. Appl. Phys. **37**, 3567 (1966).

[44] W. L. Bond, W. P. Mason, H. J. McSkimin, K. M. Olsen, and G. K. Teal, Phys. Rev. **78**, 176 (1950).

[45] J. Vallin, M. Mongy, K. Salama, and O. Beckman, J. Appl. Phys. **35**, 1825 (1964).

[46] H. J. McSkimin, W. L. Bond, E. Buehler, and G. K. Teal, Phys. Rev. **83**, 1080 (1951).

[47] F. Soyalp and G. Ugur, Philos. Mag. **91**, 468 (2010).

[48] A. F. Wright, J. Appl. Phys. **82**, 2833 (1997).

[49] A. G. Beattie and G. A. Samara, J. Appl. Phys. **42**, 2376 (1971).

[50] M. J. Tambe, N. Bonini, and N. Marzari, Phys. Rev. B **77**, 172102 (2008).

[51] K. Marklund and S. A. Mahmoud, Phys. Scr. **3**, 75 (1971).

[52] T. Lee, K. Ohmori, C. S. Shin, D. G. Cahill, I. Petrov, and J. E. Greene, Phys. Rev. B **71**, 144106 (2005).

[53] T. Soma, T. Itoh, and H. Kagaya, Phys. Status Solidi B **125**, 107 (1984).

[54] R. Tubino, L. Piseri, and G. Zerbi, J. Chem. Phys. **56**, 1022 (1972).

[55] R. Stedman and G. Nilsson, Phys. Rev. **145**, 492 (1966).

[56] Z. Jian, W. Xin, W. Guanghong, Z. Kaiming, and X. Xide, J. Phys.: Condens. Matter **8**, 6323 (1996).

[57] W. G. Stirling, J. Phys. C **5**, 2711 (1972).

[58] M. Sangster, G. Peckham, and D. Saunderson, J. Phys. C **3**, 1026 (1970).

[59] E. I. Isaev, S. I. Simak, I. A. Abrikosov, R. Ahuja, Yu. Kh. Vekilov, M. I. Katsnelson, A. I. Lichtenstein, and B. Johansson, J. Appl. Phys. **101**, 123519 (2007).